AN INVESTIGATION OF THE SPEED OF THE SOLAR DISTURBANCES RESPONSIBLE FOR TYPE III RADIO BURSTS

By J. P. WILD,* K. V. SHERIDAN,* and A. A. NEYLAN†

[*Manuscript received August* 3, 1959]

Summary

The paper describes an investigation aimed at finding out whether solar radio bursts of spectral type III are due to disturbances which travel out through the corona with velocities exceeding $0 \cdot 1c$, as predicted by the well-known hypothesis that the emissions are due to plasma oscillations. If the proposition is correct, emissions at different frequencies would be generated at different levels in the corona—the lower the frequency the higher the source. This property is tested by simultaneous directional observations at a number of frequencies between 40 and 70 Mc/s, using a swept-frequency interferometer.

The system and performance of the interferometer are described, and errors in position-finding due to ionospheric refraction are discussed.

Results for type III bursts show that different frequencies are generated at different levels in the corona according to the predicted sequence ; they therefore strongly support the plasma hypothesis. It is concluded that the corona is considerably denser in the regions where type III sources are generated than in the average corona as depicted by conventional models ; and an origin in coronal streamers is suggested.

The derived velocities of type III disturbances are found to be considerably greater than those previously deduced from spectral data alone. The range of velocities now inferred extends from $0 \cdot 2c$ to $0 \cdot 8c$, with an average of $0 \cdot 45c$. The significance of these very high velocities is discussed. For this purpose new evidence is discussed relating to the " type V " continuum emission which follows certain type III events. The combined type III–V events, which are known to correlate closely with chromospheric flares and sub-flares, are interpreted in terms of streams of relativistic electrons with energies $\gtrsim 2$ MeV which travel along magnetic lines of force in spiral paths. It is suggested that, in its outward passage, such a stream excites plasma oscillations in the surrounding coronal gas (yielding the type III burst), while, under favourable circumstances, the electrons themselves emit synchrotron radiation (yielding the type V burst.) A possible connexion between the energetic solar electrons and the corpuscular radiation surrounding the Earth is suggested.

I. INTRODUCTION

Bursts of spectral type III, which on many days dominate the records of solar activity in the metre-wavelength spectrum, are recognized by the rapid drift in the frequency of maximum intensity from high to low frequencies (Wild and McCready 1950). The earliest spectral observations showed that the frequency drift could be interpreted as a very fast outward movement of a disturbance through the solar corona ; the outward velocity was calculated

* Division of Radiophysics, C.S.I.R.O., University Grounds, Chippendale, N.S.W.

† Division of Radiophysics, C.S.I.R.O. ; present address : Mount Stromlo Observatory, Canberra.

to be in the range 3×10^4 to 10^5 km/sec, i.e. one-tenth to one-third the velocity of light (Wild 1950). This interpretation was based on the *plasma hypothesis*, namely, that the radio emission was due to plasma oscillations excited in the coronal gas surrounding a suitable kind of localized disturbance. Since the plasma frequency decreases with height in the solar corona, the observed drift from high to low frequencies corresponds to an outward movement of the disturbance. The quantitative conversion of frequency drift to velocity was made using a standard empirical model of the solar corona.

This interpretation was not taken particularly seriously until subsequent observations revealed that in some type III bursts the sources radiated in two bands corresponding to a fundamental frequency and its second harmonic: this strongly suggested that plasma oscillations were responsible (Wild, Roberts, and Murray 1954). However, since the deduced velocities are far in excess of those of any known optical phenomenon, it is obviously important to test their validity by direct means.

In the present paper* we describe an experimental test of the hypothesis using directional observations. The hypothesis predicts that, when a type III source is ejected outwards from near the limb of the Sun, the radio source should appear beyond the limb and its angular displacement from the limb should increase as the frequency decreases. This prediction is tested using a swept-frequency interferometer capable of measuring the east-west coordinate of the source position as a function of both time and frequency.

The instrument is described in Section II. Its principal limitation is imposed by the effects of ionospheric refraction, and a discussion of these effects is therefore given in Section III. The experimental results on type III bursts are presented and interpreted in Sections IV, V, and VI. Section VII gives a description and interpretation of bursts of spectral type V which frequently accompany type III bursts; this discussion is a necessary preliminary to Section VIII, where the physical nature of the type III bursts is considered.

The interferometer described in this paper is operated in conjunction with the Dapto solar radio-spectrograph whose frequency was initially 40–210 Mc/s, and is now 24–210 Mc/s. Much of the discussion of results depends on combining observations made with the two techniques.

Sample spectra of type III bursts are shown in Plate 1 and some properties of type III bursts are listed below. The quantities given apply at frequencies around 100 Mc/s unless otherwise stated, although the spectral type has been recognized over a wide frequency range between about 20 and 600 Mc/s.

Rate of frequency drift	20 Mc/s per sec
Instantaneous bandwidth	10–100 Mc/s
Duration of single burst	3–10 sec
Duration of group ($\sim$10) of bursts	$\frac{1}{2}$–2 min
Maximum intensity	$\sim 10^{-18}$ W m^{-2} (c/s)$^{-1}$

* A preliminary sample of the results of this paper was discussed at the Paris Symposium on Radio Astronomy 1958 (Wild, Sheridan, and Trent 1959).

Apparent angular size	~6 min of arc at 65 Mc/s, increasing with decreasing frequency (see Wild and Sheridan 1958)
Polarization	Varies between random and strongly circular or elliptical (Komesaroff 1958)
Frequency of occurrence	Up to several groups per hour at times of strong activity
Optical correlation	Marked correlation with solar flares and micro-flares (Lough-head, Roberts, and McCabe 1957). The bursts occur close to the time when the flare shows its initial sudden expansion (Giovanelli 1958).

II. The Swept-frequency Interferometer

The function of the interferometer used in this investigation is to measure one coordinate (parallel to the observer's east-west line) of the centroid of an isolated source situated on or near the Sun's disk. The measurement can be made effectively simultaneously at five to ten different frequencies between 40 and 70 Mc/s at successive times separated by $\frac{1}{2}$ sec. The accuracy of measurement is about ± 1 min of arc.

The principles of operation and technical details of the swept-frequency interferometer in its initial form have been discussed in a previous paper (Wild and Sheridan 1958). Major features have since been added as a result of operating experience. Firstly, an additional interferometer system with a short base line has been incorporated for lobe identification. Secondly, a more convenient display system has been used and an automatic system of "following" and calibration has been incorporated. The latter facilities have resulted in a reduction, by an order of magnitude, of the time required to analyse the records, which is a major factor in the feasibility of the experiment.

In the outline of the whole system given below, emphasis will be given to the new features. A simplified diagram of the system is given in Figure 1.

(*a*) *The Principle of Position Measurements*

Two aerials, 1 km apart on an east-west line, are connected to a central receiver whose frequency is swept twice per second through the range 40–70 Mc/s. The relative length of the aerial feeder lines is capable of extensive variation in steps of 15 m ; it is regulated throughout the day in such a way that the excess length s of the path travelled by signals coming from the direction of the centre of the Sun's disk via the west aerial over that via the east aerial is constrained to lie within the limits $45\text{ m} \leqslant s \leqslant 60\text{ m}$. This regulation is controlled by a computor which is described later.

It is readily seen that a broad-band source of emission situated at the centre of the Sun's disk will induce coherent signals in the two aerial channels, and that when added together the envelope of the instantaneous spectrum that would be given by either one of the channels alone now becomes modulated by an interference pattern, whose maxima occur at the frequencies

$$f_n = n(c/s),$$

where c is the velocity of light and n assumes integral values. For a source whose centroid lies a small angular distance, φ radians, east of centre, the frequency of maxima are given by

$$f_n = nc/(s + a'\varphi),$$

where a' denotes the foreshortened base line of the interferometer as viewed from the direction of the Sun.

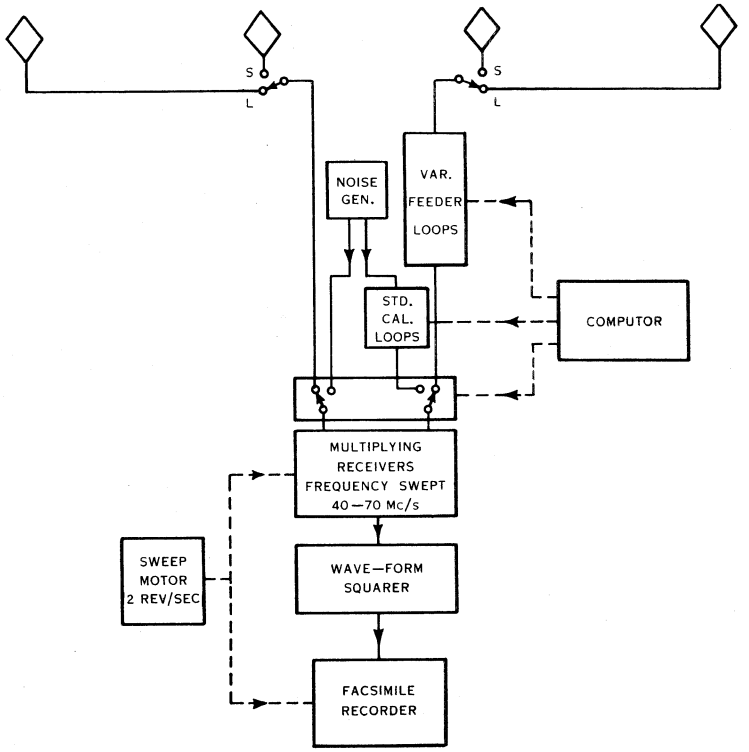

Fig. 1.—Simplified block diagram of the swept-frequency interferometer. Short-base and long-base interferometers are selected by the S/L switch.

In practice the signals in the two channels are combined by a process of multiplication rather than addition, and hence the output " spectrum " consists of the modulation pattern alone, i.e. positive and negative swings in the interference pattern are symmetrical about the zero line. Under the adopted conditions the zero line is crossed at five to ten frequencies (given by $f_n \pm \frac{1}{4}$) and so, if means are provided to determine the correct lobe number n, the angle φ can be measured at each of these frequencies.

(*b*) *The Method of Display*

In the new system of display each swept-frequency modulation pattern delivered by the interferometer is converted into a square waveform (by passing the waveform through a high-gain amplifier that cuts off the extremities of the positive and negative swings) and displayed as a single intensity-modulated line on paper records using a facsimile recorder.* Successive traces at $\frac{1}{2}$ sec intervals are recorded one below the other, partially overlapping, as in ordinary records of dynamic spectra. Each zero point can then be recognized as a sudden change between a black and a white region.

Figure 2 represents an idealized record of a solar source; the first part (between 1159 and 1203 local apparent time) shows a broad-band source *fixed* on the Sun's disk, the second (between 1203·5 and 1204·5) a source which changes position and becomes dispersive with time. Between 1159 and 1200 the swept-frequency pattern gradually drifts and expands owing to the decrease in s with the westward movement of the Sun through the sky. At 1200, s has decreased to 45 m, at which stage the relative feeder length is automatically changed to make $s=60$ m. The new compressed pattern then proceeds to expand again until s has once again decreased to 45 m at about 1203·5. This procedure is repeated continually throughout the observing period. Of course, the record appears banded only when sufficiently intense solar radiation is being received; at other times it consists of random noise.

(*c*) *Calibration of the Record*

In the method used to analyse the records, the first step is to generate a reference pattern, superimposed on the actual paper record, corresponding to a source situated precisely at the centre of the Sun's disk. To do this, the pair of aerial feeders are, at precisely controlled intervals of time, automatically disconnected from their receiver terminals and replaced for a few seconds by a pair of calibration lines connected to a broad-band noise generator. The latter delivers along the calibration lines a pair of mutually isolated but phase-coherent noise signals. The lengths of the two calibration lines are identical, except that one of them contains an additional loop of length l appropriate to the position of the centre of the Sun at that instant of time. By this means the pattern due to a central solar source is completely simulated. In practice, four standard l-values are used for calibration, namely 60, 55, 50, and 45 m; thus the extreme values are used at the beginning and end of each main switching period. The

* Facsimile recorders were developed primarily for the reception of newspaper photographs transmitted by radio. Electro-sensitive recording paper (9 in. wide in the present case) is fed between and in contact with two stainless steel electrodes. One electrode is a thin bar extending across the width of the paper; the other is a single-turn helical wire mounted on a cylindrical former whose axis extends across the width of the paper. Rotation of the helix through one revolution sweeps the point of contact with the paper from one side to the other. The signal is applied as a potential difference between the electrodes. The electrolytic current flowing at any instant between the electrodes deposits ferric ions into the paper, causing it to blacken in the appropriate spot with a density which increases with the current. The recorder used in this experiment was the product of Hogan Laboratories, New York.

appropriate times at which the calibrations are inserted are calculated by a clock-driven computor described below.

The calibration patterns appear in Figure 2 as brief sections of extra blackness. The continuous pattern corresponding to a central solar source is then given with sufficient accuracy by joining adjacent calibration marks by straight lines, shown dashed in the figure. It is then a simple matter to measure the time displacement between the actual pattern and the reference pattern, and hence determine φ at any desired frequency and time (see Section II (f)).

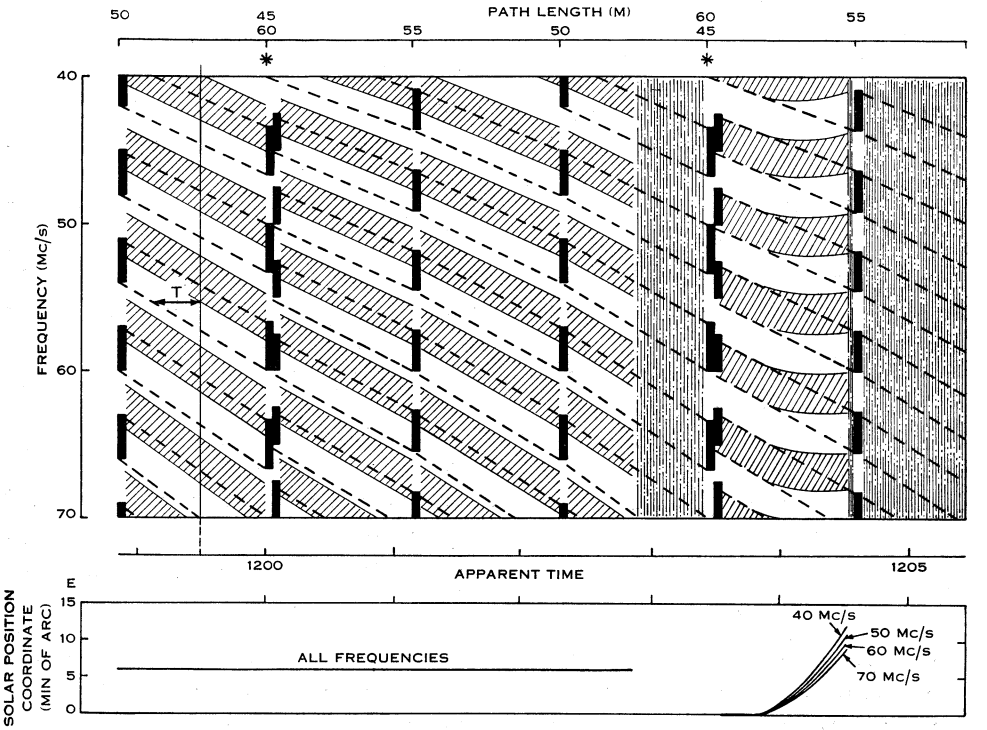

Fig. 2.—Idealized record obtained with the swept-frequency interferometer. The hatched bands, which appear black on the actual record, are produced by a hypothetical solar source, whose position is shown in the lower part. The dotted lines are drawn manually on the record by joining the appropriate calibration marks. The asterisks indicate times at which the relative lengths of the aerial feeder lines are changed by 15 m.

Rapid movements in the position of a source can be recognized by inspection, as illustrated in the latter part of Figure 2. In the example given, the source is initially at the centre of the Sun and all frequencies arrive from this direction. As it moves outwards towards the east, different frequencies are shown arriving from different directions.

(*d*) *The Computor*

Let us designate by l' the difference in the path length travelled by plane waves arriving from the direction of the centre of the Sun's disk to the two *aerials* of the interferometer. Then the system described above requires a computor

which delivers pulses at those times when, for integral values of p, l' assumes the values :

(i) $l'=p\times 15$ metres, for the purpose of changing the relative lengths of the aerial feeder lines in steps of 15 m, and

(ii) $l'=p\times 5$ metres, for the purpose of controlling the calibration system.

Clearly, a system that satisfies (ii) can be made to satisfy (i) also by selecting every third pulse.

Now, for an east-west interferometer, l' is given by the well-known equation

$$l'=a\sin H\cos\delta,$$

where a is the distance between aerials, H the hour angle, and δ the declination of the centre of the Sun's disk. Hence to satisfy (ii), we require pulses to be delivered at times corresponding to the hour angles H_p given by

$$\tfrac{1}{5}a\sin H_p\cos\delta=p,$$

where a is measured in metres. The declination δ changes only slowly with time, and for present purposes can be regarded as constant throughout one 4-hr period of observation. For a reason which will become apparent, let the last equation be written in the form

$$\{(\tfrac{1}{5}a/A)\cos\delta\}(A\sin H_p)=p,$$

where $A=1{\cdot}3750\times 10^4$.

To produce the desired sequence of pulses (see Fig. 3) we have made use of a small commercially available hand calculator (*Curta*) which is capable of adding a number to itself m times, with an accuracy exceeding 1 in 10^7, by m rotations of a shaft. The number $(\tfrac{1}{5}a/A)\cos\delta$ (appropriate to the daily value of δ) is set up on the calculator and the shaft is driven at a variable rate such that the cumulative number of revolutions measured from noon is $A\sin H$. The cumulative product, $\tfrac{1}{5}a\cos\delta\sin H$, therefore appears on the register, and arrangements are made for a pulse to be delivered when the digit corresponding to integral values of p changes its value.

The variable drive of the computor shaft is achieved by using a constant-speed, crystal-controlled, synchronous motor driven at the rate $A(\mathrm{d}H/\mathrm{d}t)$, which is exactly 1 rev/sec with the chosen value of A. This is the maximum driving rate required, and indeed approximates closely to the required rate during a considerable period around noon, since then $H\approx\sin H$. The motor is normally connected to the calculator's shaft, but it is occasionally declutched for exactly one revolution at times determined by a *standard* programmed tape to compensate for the difference between AH and $A\sin H$ in the cumulative number of revolutions. The interferometer is operated daily for about 4 hr centred on noon, and during this time the motor makes some 10^4 revolutions, of which less than 10^3 are declutched. The computor delivers pulses with an accuracy of about ± 1 sec.

(*e*) *The Complete Record*: *Ambiguity Resolution and Polarization*

Figure 4 shows an actual record taken during a period of prolonged, broad-band, intense emission from the Sun. It contains the basic features shown in the idealized record of Figure 2 (viz. the patterns due to the source and calibration signals), but contains additional information of two kinds.

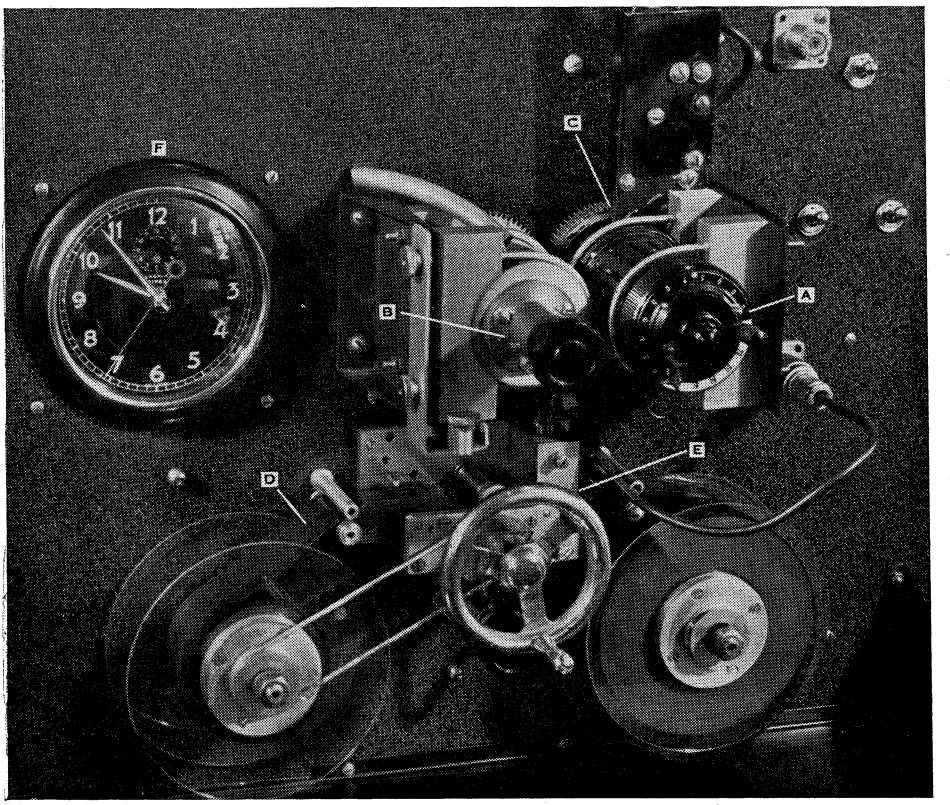

Fig. 3.—The computor used to control the interferometer. A digital calculator *A* is driven by a synchronous motor (behind panel) *via* a magnetic clutch *B*. The appropriate shaft of the calculator operates a photoelectric switch *C* to deliver the output pulse. The magnetic clutch is controlled by a photoelectric switch *E*, which is operated by a programmed tape *D*. The clock *F*, which is set to read local apparent time, is mechanically coupled to the programmed tape.

Firstly, there are periods of about 3 sec (selected by the operator) during which the aerials of the short-base ($\frac{1}{4}$ km) interferometer are substituted for those of the long-base one. As previously intimated, this information is essential to identify the correct lobe (i.e. the correct dark band on the record) associated with the long-base interferometer. While the lobe separation of the long-base system is only about 20 min of arc, that of the short-base system is about 80 min of arc, i.e. sufficiently great to avoid confusion in all but exceptional cases.

The ratio of the two base lines is made equal to $4 \pm 0 \cdot 0001$. It can be shown that this choice allows the same computor etc. to be used for both systems:

in the case of the short-base system the feeder-line switching is controlled by a " memory system " that takes note only of every fourth pulse fed to the long-base system, and similarly the record analyst takes note only of every fourth calibration on the record. In practice the operator can change from long- to short-base operation by pressing a switch which interchanges the aerials and automatically resets the aerial line lengths.

The second additional facility shown on the record is the provision of short periods of a few seconds (again selected by the operator), during which the rhombic aerials of the normal interferometer are replaced by a pair of coaxial

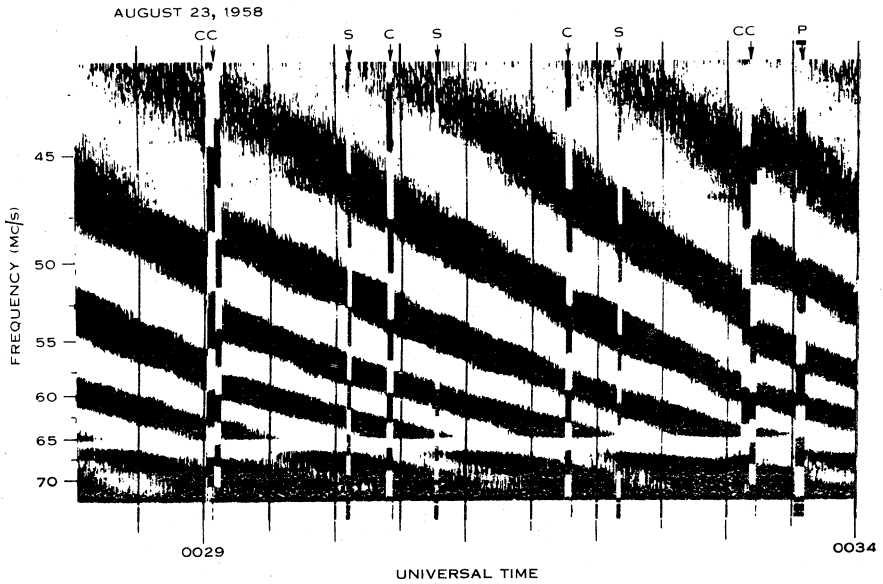

Fig. 4.—Photographic reproduction of an actual facsimile record obtained with the swept-frequency interferometer during a prolonged solar radio storm. The interferometer is operated with the receiver connected to the long-base (1 km) aerial system except for short intervals indicated as follows: *S*, short-base ($\frac{1}{4}$ km) system; *P*, polarization aerial system; *C*, calibration system. The horizontal bands between 65 and 70 Mc/s are due to interference from television stations.

rhombics with mutually perpendicular planes of polarization. These are connected to the receiving system through lengths of line that differ by a fixed amount (45 m), and cause a swept-frequency interference pattern to be generated when coherent signals are received in the two aerials. Measurement of the phase of this pattern yields information on the type of *polarization* (random, circular, linear, or elliptical) being received. The system is essentially similar to that described by Komesaroff (1958) but the accuracy of phase measurement is enhanced by the use of the multiplying receiving system and improved display. Information on polarization will not be discussed in the present paper.

Records of type III bursts, where the coherent interferometer pattern appears only for brief periods of time, are basically similar. Examples are shown in Figure 5.

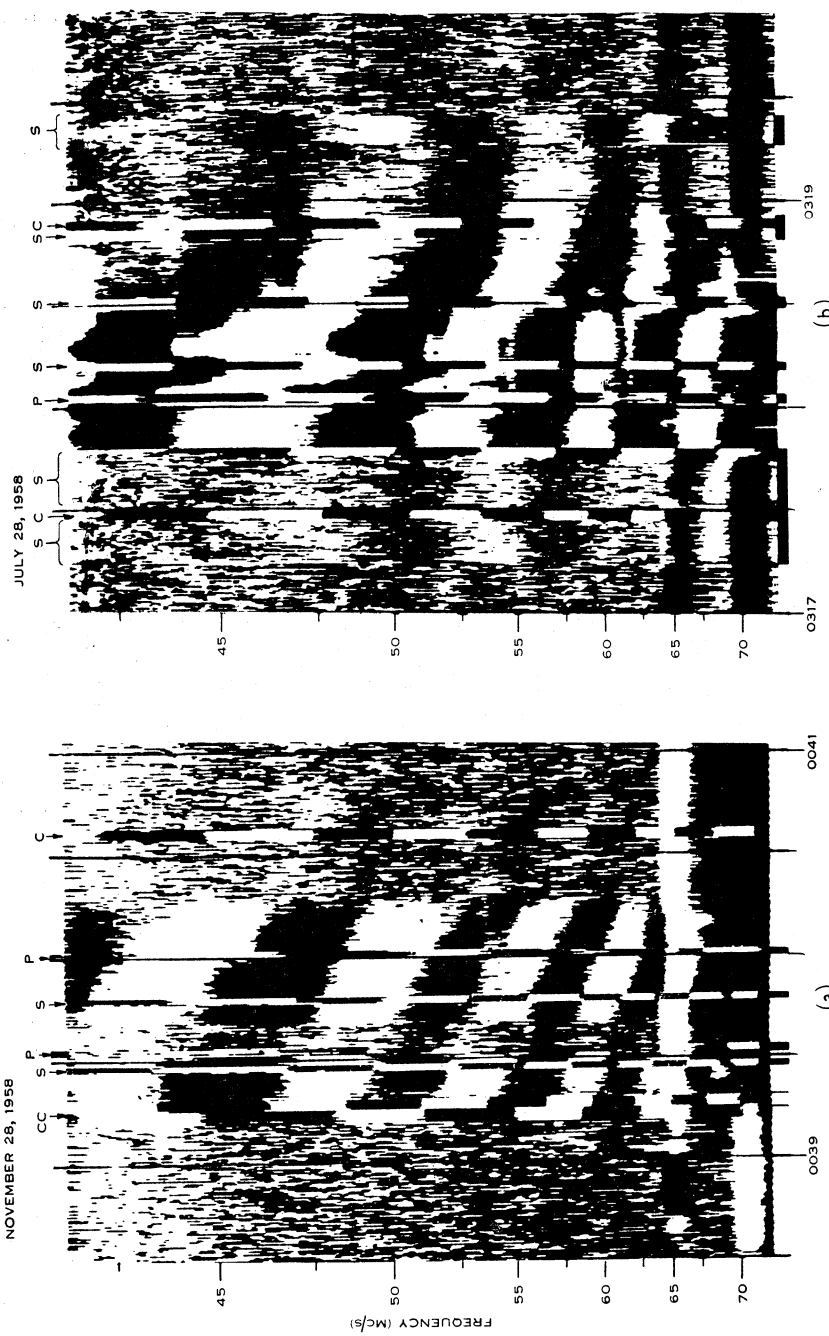

Fig. 5.—Interferometer records of groups of type III bursts. (*a*) is a "normal" record, in which the position at a given frequency remains constant, while (*b*) is an extreme example in which the position shows rapid changes. Details are as in Figure 4.

(*f*) *Analysis of the Records*

The procedure for analysing records of type III bursts consists of the following steps :

(i) Corresponding calibration points are joined on the paper by pencilled lines, so as to give the pattern corresponding to a central solar source. This is performed for both the long-base system (in detail) and the short-base system (as necessary).

(ii) At a selected time during the life of the bursts (or more than one time if source movements are evident), the time delay T between the actual source and calibration source may be read at each frequency defining the edge of a black band. Measurement of the quantity T is illustrated on the left-hand side of Figure 2. Now it is clear that if T is positive (in the sense that a point on the pattern of the actual source *follows* the corresponding one on the calibration source, as in Fig. 2), then the source must have drifted through the appropriate interferometer lobe *after* the centre of the disk, i.e. the source is east of centre. Further, it may simply be shown that the magnitude of the angular position coordinate φ is then given in radians by*

$$\varphi=\frac{\cos H\cos\delta}{\sqrt{(1-\sin^2 H\cos^2\delta)}}\frac{\mathrm{d}H}{\mathrm{d}t}T.$$

In practice the quantity φ, rather than T, is read directly from the record by using a " slide-rule " device to make the numerical conversion. Values of φ can be determined at about ten frequencies for a given time.

(iii) To standardize the frequency values, the results are expressed in terms of averages within five adjacent frequency bands. These bands are 5 Mc/s in width, and centred on the standard values 45, 50, 55, 60, and 65 Mc/s. (The 65 Mc/s is often unreliable owing to interference from television signals.)

(iv) The final results required for solar purposes are conveniently expressed in terms of the *position coordinates*, P_{45}, P_{50}, P_{55}, P_{60}, and P_{65}, at the five frequencies. This quantity is defined as the projected distance (normally measured in units of the photospheric radius R_0) between the centre of the disk and the source, measured in the terrestrial east-west direction. It is evident that the position coordinate is given by

$$P_f=(R_0/\Omega)\varphi(f),$$

where Ω is the semi-angle subtended by the photosphere at the Earth.

* This may be derived from Section IV *A* (2) of Wild and Sheridan (1958), subject to the note below, or more directly from first principles.

Note.—We take this opportunity of correcting an error in the section cited in the above paper. In Figure 11 of that paper, ΔH should be replaced by $\Delta H\cos\delta$, and equations (**10**)–(**14**) modified accordingly. Using the notation of that paper (e.g. r for the present φ), the final equations (**13**) and (**14**) should read, respectively :

$$r=(\sin\theta-\sin H_0\cos\delta_0)(1-\sin^2 H_0\cos^2\delta_0)^{-\frac{1}{2}},$$
$$\psi=\pm\tan^{-1}(\tan H_0\sin\delta_0).$$

For some purposes (e.g. optical identifications) it is also required to specify the orientation of the lobes on the solar disk. This is given by the angle ψ between the lobes and the solar diameter through the north point of the Sun at noon, thus*

$$\tan \psi = \pm \tan H \sin \delta.$$

(*g*) *An Empirical Correction*

The correct functioning of the interferometer depends on each radio-frequency line and loop of the system possessing its assigned electrical length and sufficient uniformity to avoid unwanted phase errors. The measures taken to meet these requirements were described by Wild and Sheridan (1958). An excellent test of the whole system is provided by observations of reasonably static solar radio storms that continue throughout a 4-hr observing period. Such records were examined closely for signs of instrumental defects, e.g. sudden changes in apparent positions at times when the line lengths were switched. With one exception, such changes were found to be entirely absent within the accuracy of measurement (± 1 min of arc). The exception referred to positions in the 60 Mc/s band, which invariably showed a sudden change of 5 min of arc at noon, when the main loop system was transferred from the eastern to the western line. This error is believed due to the cumulative addition of phase errors in the 15 m loop system which would occur at harmonics of 20 Mc/s. A uniform correction of 2·5 min of arc was therefore applied to all 60 Mc/s positions, westward before noon and eastward after. The efficacy of this correction may be judged from inspection of Figure 6, now to be discussed.

III. Ionospheric Refraction

A serious threat to the success of the experiment is imposed by the unknown errors in position measurement caused by refraction in the ionosphere of the incident solar radiation, particularly irregular refraction. Since the angular deviation caused by refraction at an ionospheric gradient increases approximately with the square of the wavelength, it is desirable to design the experiment in the first place so as to observe at the highest acceptable frequencies. The reasons for choosing a frequency range as low as 40–70 Mc/s have been discussed previously (Wild and Sheridan 1958). Briefly, they depend on (1) a desire to observe the fundamental frequency emitted in type III bursts ($f \lesssim 90$ Mc/s) and (2) the fact that the effect we are looking for is itself more pronounced at low frequencies. We must therefore be resigned to the troublesome effects of ionospheric distortion.

A convenient comprehensive test of ionospheric effects is again provided by observations of the relatively stable solar sources responsible for storms of long duration. A reduced record of such a storm is shown in Figure 6 (*a*). At any one time all frequencies appear to arrive from the same position to within about ± 2 min of arc and this position changes only slightly during the course of the storm. This movement appears to be solar rather than ionospheric in

* See previous footnote.

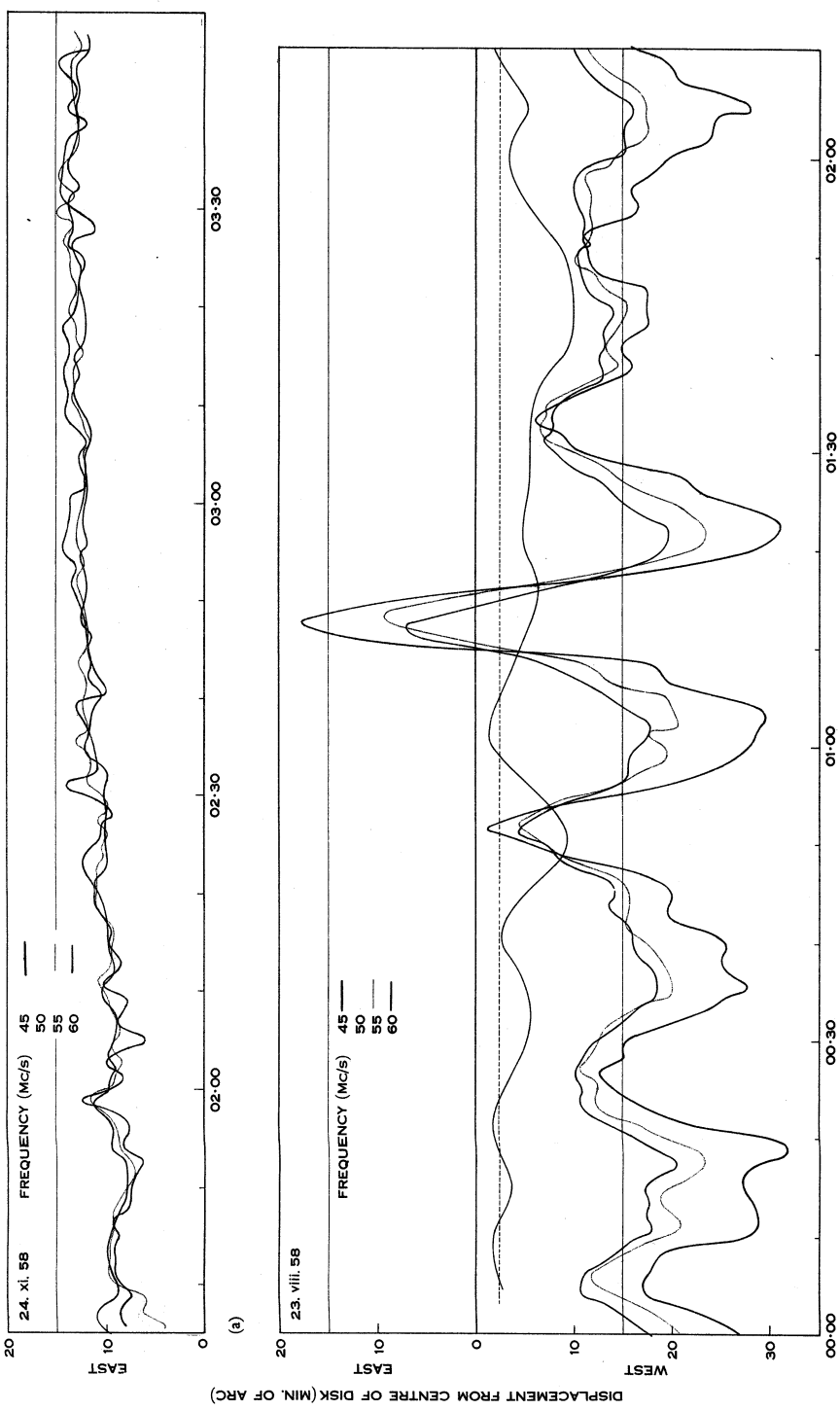

Fig. 6.—The variation of source position with time at four frequencies during prolonged solar radio storms. In (*a*) all frequencies arrive simultaneously from about the same position. In (*b*) there are large, quasi-periodic variations which are believed due to ionospheric refraction. The full black line shows the position of the unrefracted source if certain simplifying assumptions are made. The dotted black line shows the optical position of the centre of the sunspot believed responsible for the emission.

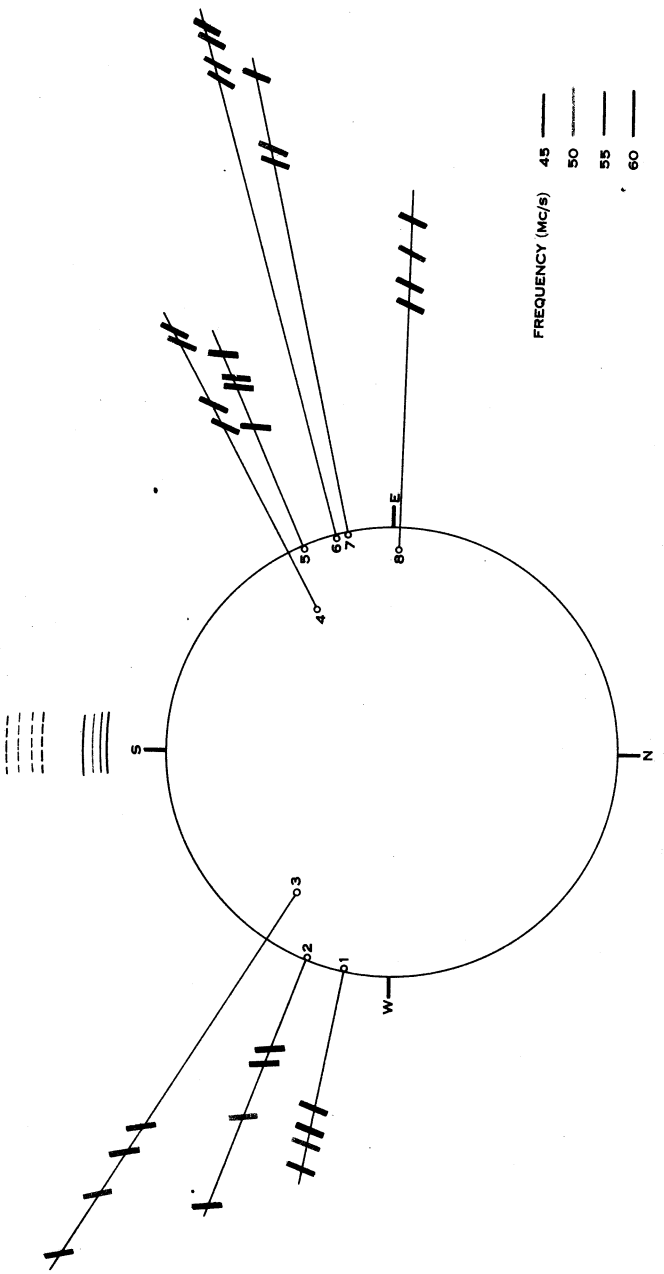

Fig. 7.—The source positions of eight type III bursts (coloured lines) associated with limb flares (optical positions shown as open circles). The lines on which the radio sources are located by the interferometer are shown in part only, viz. that part which is close to the radial line drawn through the optical flare. The circular arcs show the levels of the fundamental (full lines) and second harmonics (dotted lines) of the plasma frequency, assuming the Baumbach-Allen corona.

origin, since refraction would cause a systematic dispersion of positions with frequency. We may therefore conclude that on such occasions ionospheric effects are quite unimportant.

In contrast to this behaviour, records are also obtained in which the position swings wildly from side to side. An example is given in Figure 6 (*b*), where deviations of as much as 20 min of arc are present. The amount of deviation depends on frequency in a remarkably systematic way—the lower the frequency the greater the deviation. This is qualitatively consistent with the effects to be expected from ionospheric refraction. To test this quantitatively, let us attempt to fit the data to a scheme depending on two simplifying assumptions: (1) that all frequencies emitted by the source originated from the same position at any one time as in Figure 6 (*a*), and (2) that the deviations are due to refraction in a slowly varying, " thin " ionospheric wedge. Then it can simply be shown that the angular position coordinate at frequency f is given by

$$\varphi(f)=\varphi(\infty)+kf^{-2},$$

where k is independent of f but varies with the gradient of the refracting wedge. Evidently, $\varphi(\infty)$ is the true position of the source. A plot of $\varphi(f)$ versus f^{-2} at any instant should therefore give a straight line which intersects the $\varphi(f)$ axis at $\varphi(\infty)$. The procedure was applied to Figure 6 (*b*) at time intervals of 5 min. It was found that in most cases a straight line could be drawn through each set of observational points on the plot of $\varphi(f)$ versus f^{-2}. The consequent values of $\varphi(\infty)$ are indicated by the full black line. This may be compared with the dotted black line which shows the position coordinate of the centre of a large sunspot which was almost certainly responsible for the storm. Bearing in mind the obvious oversimplification of the initial assumptions, the relatively small difference between the two black lines strongly suggests that the observed deviations in the radio positions are mainly due to ionospheric refraction.* When such conditions prevail, observations of the positions of individual short-lived solar phenomena may be seriously in error. Such errors are a likely contributory cause of the scatter component in the statistical analysis discussed below in Section IV (*b*) (ii).

IV. Position Measurements of Type III Bursts

The observations presented here were made between June and December 1958, and the analysis is based on about 100 groups of type III bursts.

(*a*) *The Variation of Position with Time at a Given Frequency*

Inspection of the unreduced records showed that in the majority of cases the position at any given frequency remained constant to within about ± 1 min

* The quasi-periodic nature of the positional variations evident in Figure 6 (*b*) may be of considerable interest in ionospheric studies. The period is about 22 min; in another record taken on July 13, 1958, a similar periodicity was present. This periodicity seems to indicate a very large-scale structure in the irregular ionosphere. Assuming the time variations to be due only to the rotation of the ionosphere through the line joining Sun and observer (i.e. zero " wind " velocity) and also that the refraction occurs at a height of 200 km, we deduce a periodic variation in the irregular ionosphere with scale size about 25 km.

of arc throughout the lifetime of an individual burst. Also bursts of a group were usually located in the same position (e.g. Fig. 5 (*a*)). Exceptions to this rule sometimes occurred (e.g. Fig. 5 (*b*)) when the position appeared to dart about between two or more fixed positions.

(*b*) *The Variation of Position with Frequency*

In general the position of a type III source showed systematic variations with frequency. This question is critical in testing the validity of the plasma hypothesis, and it is interesting to consider first the most direct test of the hypothesis, i.e. to examine the radio positions of events associated with chromospheric flares situated near the limb.

(i) *Events associated with Limb Flares.*—The identification of flares associated with type III bursts is a procedure which requires considerable caution. Both flares and bursts tend to be numerous on the same days, and the probability of chance coincidences is high. We have therefore counted only those cases in which (1) the burst occurs between the start and maximum of the flare and (2) both burst and flare are so isolated that confusion is extremely unlikely. On this basis eight limb-flare events were recognized.* The optical and radio positions are shown in Figure 7 ; each radio position is presented as a small section of the line on which the centroid of the source is located by the interferometer, viz. the section centred on the radial line through the flare.

In each case the radio positions are seen to lie beyond the optical limb, and the distance from the centre increases systematically with decreasing frequency. Since higher frequencies invariably arrive before lower frequencies in type III bursts, these results strongly support the hypothesis that the different frequencies originate at different levels in the path of a disturbance travelling outwards through the solar corona. If it is assumed that the path of the disturbance is in fact radial and that the relative positions are not distorted by refraction, we can combine the positions of Figure 7 with the corresponding drift rates given by the dynamic spectra to calculate the velocity of the disturbance. Velocities thus calculated are found to lie in the range $\frac{1}{4}c$ to c. These values are considerably greater than those previously inferred from spectral data.

(ii) *Statistical Analysis of Radio Positions.*—The *spread* of position with frequency, clearly evident in Figure 7, is examined in Figure 8 (*a*) using the complete set of radio observations. The purpose of the figure is to investigate statistically how the amount of spread varies with position on the Sun. Thus the abscissa represents the position coordinate at 60 Mc/s and the ordinate the difference between the position at 60 Mc/s and that at 45 Mc/s. Each dot represents an observed burst or homogeneous group of bursts. Roughly, the points are seen to be scattered about a straight slanting line passing through the origin. Hence we shall refer to this diagram in terms of two components—the *linear* and *scatter* components.

* The optical data on flares was kindly supplied by Dr. R. G. Giovanelli and Miss M. McCabe of the Division of Physics, C.S.I.R.O., to whom the authors are obliged for much helpful cooperation.

The linear component is shown in Figure 8 (*b*), in which mean values of the ordinates of Figure 8 (*a*) have been plotted for successive narrow ranges of the abscissa. It may be interpreted in terms of the simple model shown in Figure 9, where different frequencies are assumed to originate at different fixed levels in the solar atmosphere. In the idealized case, when refraction is negligible and when the lobes of the interferometer pattern lie normal to the plane of the figure, it is readily seen that the spread (P_{45}–P_{60}) is a linear function of position (P_{60}).

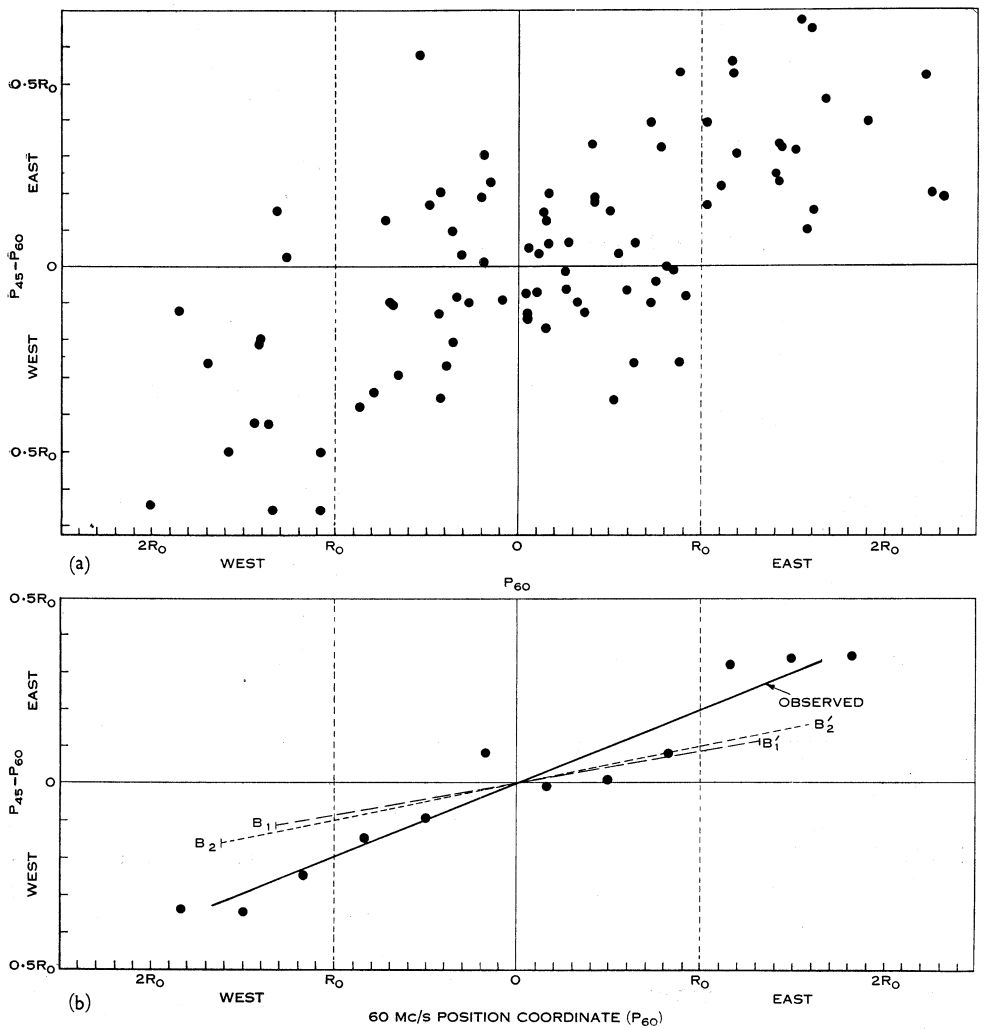

Fig. 8.—Showing the distribution with 60 Mc/s position on the disk of the amount of the " position spread " in type III bursts (as measured by the difference between 45 and 60 Mc/s position co-ordinates). In (*a*) each burst or group of bursts is shown as a dot. In (*b*) the mean positions in each abscissa-group are shown. The line through the observed points is compared with that predicted by the plasma hypothesis assuming the Baumbach-Allen corona. The predicted lines refer to sources originating at the fundamental plasma frequency (B_1B_1') and at the second harmonic of the plasma frequency (B_2B_2').

Thus the presence of a systematic (linear) component in Figure 8, which contains ten times as many events as Figure 7, provides further evidence that different frequencies originate at different levels. Moreover, the gradient and extent of this line can be used to obtain information on the electron density distribution of the solar corona (see Section V (*b*)).

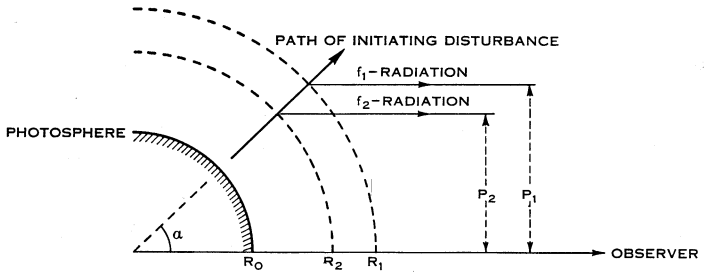

Fig. 9.—Idealized diagram showing the radio emission from a radially ejected type III disturbance.

The scatter component can be due to several causes, e.g. irregular refraction in the terrestrial and solar atmospheres, variations in the heights of emission levels from event to event, variations in the angle between the path of the disturbance and the radial direction, and variations due to different angles between the path of the disturbance and the scanning direction of the interferometer.

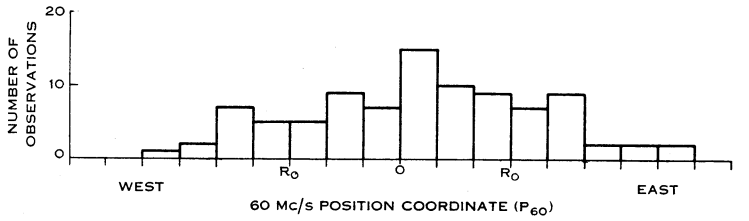

Fig. 10.—Distribution across the disk of 60 Mc/s sources of type III bursts.

The data of Figure 8 may be used to derive the approximate mean radial distances, R_{45} and R_{60}, at which sources of 45 and 60 Mc/s bursts radiate. We first plot the distribution of 60 Mc/s position coordinates (Fig. 10): the distribution is seen to be fairly uniform* between $\pm 1 \cdot 66 R_0$, where the number of events drops sharply. Hence we infer

$$R_{60} \approx 1 \cdot 66 R_0.$$

For the separation between the 60 and 45 Mc/s levels, Figure 8 (*b*) gives $R_{45}-R_{60} \approx 0 \cdot 34 R_0$ (from the value of $P_{45}-P_{60}$ at $P_{60}=1 \cdot 66 R_0$), whence

$$R_{45} \approx 2 \cdot 0 R_0.$$

* The number of events (56) on the eastern side considerably exceeds that (36) on the western side; while this difference may have arisen because the observing period was too short to be completely representative, it is certainly consistent with an effect of east-west asymmetry noted in the distribution of bursts by Hey, Parsons, and Phillips (1948), Hey and Hughes (1955), and Loughhead, Roberts, and McCabe (1957).

Finally, to investigate the velocity of the inferred travelling disturbances, we calculate the " east-west component of the apparent transverse velocity " of each event. This is given by $(P_{45}-P_{60})/(t_{45}-t_{60})$, where t_{45} and t_{60} denote the times of maximum intensity at frequencies of 45 and 60 Mc/s. Figure 11 shows how this velocity varies from centre to limb, using the 60 Mc/s position co-ordinate as abscissa. Each point represents the mean of about ten bursts, and the total length of the vertical lines through each point denotes the standard deviation. The velocity is seen to increase from about zero at the centre to about $0{\cdot}5c$ at the radio limb. Thus, neglecting the possible effects of systematic refraction, we again find evidence for radial-like disturbances with mean outward velocities of about $0{\cdot}5c$.

Discussion of velocities will be continued in Section VI.

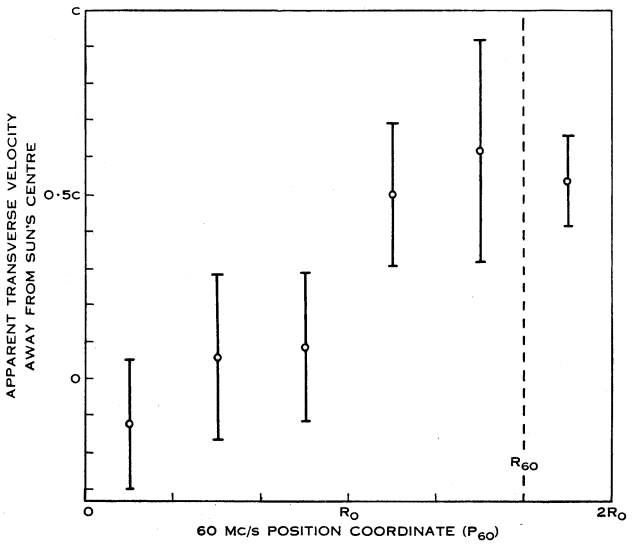

Fig. 11.—The variation with 60 Mc/s position on the disk of the transverse component of the apparent outward velocity of type III disturbances. Each point represents the mean of about ten values of independent events, and total lengths of the vertical lines signify the standard deviations.

V. Implications of the Plasma Hypothesis

The evidence given above that the height of origin of type III bursts increases with decreasing frequency strongly favours the widely accepted hypothesis that the frequency emitted from a given level in the corona is either the fundamental plasma frequency or its second harmonic. We now explore some of the consequences of applying this hypothesis to the present observations.

(*a*) *The Escape of Fundamental and Second Harmonic Frequencies*

If the solar atmosphere is assumed to be smooth and spherically symmetrical with its electron density decreasing monotonically outwards, then the fundamental plasma frequency can escape from its level of origin only along a radial path

(see Jaeger and Westfold 1950; Wild, Murray, and Rowe 1954). The second harmonic, on the other hand, is free to escape through a wide cone of angles around the radial direction. One might predict, therefore, that those type III bursts which contain *both* harmonics should be found only near the centre of the disk, and that events recorded elsewhere should be purely second harmonic.

To investigate this prediction we have plotted (Fig. 12) the distribution across the Sun of the percentage of events showing both harmonics. While the number of these events is small (20), there seems to be a definite indication of a gradual rise from centre to limb and possibly a more sudden decline beyond the limb. In the majority of these cases the fundamental was more intense than the harmonic. Thus it is found that the fundamental can escape from the whole radio disk, whence the prediction of the simple theory is directly contradicted.

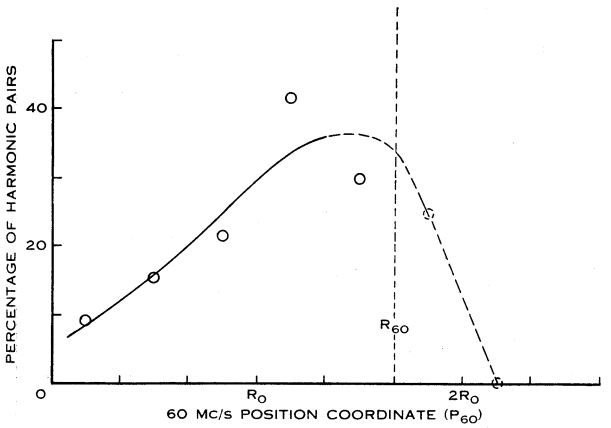

Fig. 12.—Distribution with 60 Mc/s position on the disk of the percentage of type III bursts which show recognizable harmonics.

The form of the distribution of Figure 12 could arise in the following way. The small number of recognizable harmonic pairs near the centre is caused by the second harmonic being usually swamped by the fundamental. The swamping effect gradually decreases with distance from the centre, so causing a gradual increase in the number of recognizable pairs. On the other hand the apparent absence of pairs beyond the normal radio limb could be due to the *absence* of a fundamental in events taking place very close to and actually round the limb. This interpretation is consistent with evidence given by Roberts (1959) for type II bursts which are believed to originate at the same levels as the type III bursts. In the present discussion we shall assume that, across the " normal " radio disk, the fundamental frequency dominates the second harmonic to the extent that the latter can be neglected. This assumption applies to the low frequencies in question, and is certainly not valid at high frequencies (e.g. $\gtrsim$150 Mc/s).

The escape of the fundamental plasma frequency through a wide cone of angles becomes possible if the solar atmosphere is pervaded by small-scale

irregularities (see Roberts 1959). Indeed, the existence of such irregularities seems essential to the survival of the plasma hypothesis.

The path followed by a ray escaping outwards from the plasma level through an irregular but quasi-spherical atmosphere requires detailed consideration beyond the scope of the present paper. We may merely surmise that near its start the path meanders through the highly refracting irregularities in all directions, while on the average the direction of escape is radial, i.e. the mean path is deviated *away* from the centre of the disk. Subsequently we should

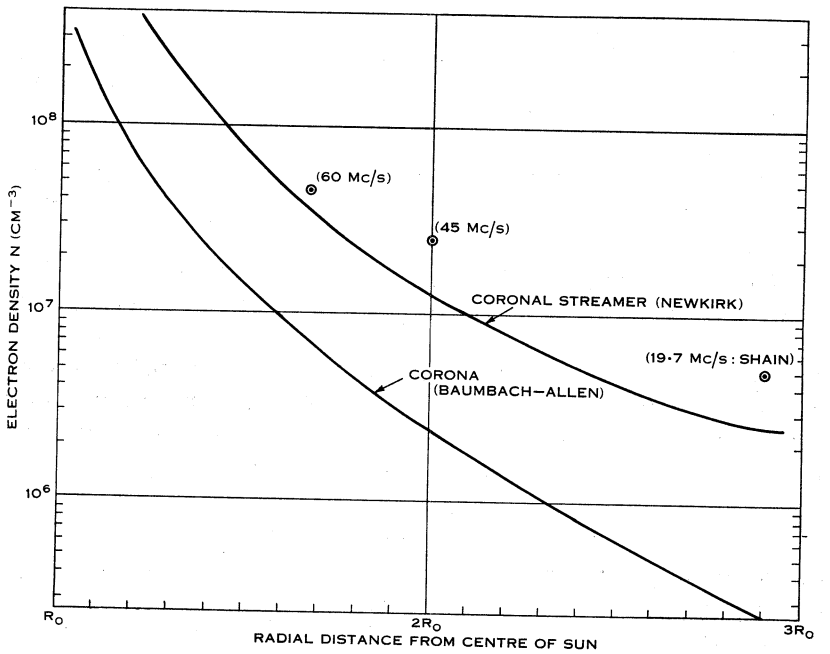

Fig. 13.—Electron densities in the solar corona as a function of radial distance from the centre of the Sun. The lower curve is the standard Baumbach-Allen model; the upper curve is that given by Newkirk for the corona above an average active centre (1956–1958). The experimental points refer to the active regions in which type III sources are generated, the latter being supposed to originate at the fundamental plasma level. The 45 and 60 Mc/s points emerge from the present analysis, while the 19·7 Mc/s point is due to Shain and Higgins (1959).

expect the path to curve *inwards* owing to the effects of spherical refraction (Jaeger and Westfold 1950). As pointed out by Shain and Higgins (1959), these two opposing effects are likely to be comparable in magnitude. For the purposes of the present discussion, therefore, it seems reasonable to make the simplifying assumption that the measurement of the position of sources located at the plasma level is unaffected by refraction in the solar atmosphere. In this connexion it is noteworthy that there is evidence for no refraction for other types of emission, believed to be broad-band emission from a fixed source (see Fig. 6 (*a*) and Wild, Sheridan, and Trent 1959).

(*b*) *The Radial Distribution of Electron Density*

The heights of several plasma levels in the " normal " corona, as represented by the Baumbach-Allen model, are shown as coloured arcs (full lines) at the top of Figure 7. These levels are seen to be considerably lower and closer together than those actually observed. The same conclusion emerges from Figure 8 (*b*), where the linear component calculated from the Baumbach-Allen model (B_1B_1') is seen to be less steep and less extended than the observed line. Thus, if the assumptions discussed in (*a*) are substantially correct, type III bursts must originate in locally dense regions of the corona.

Identifying the mean radial distances R_{45} and R_{60} (see Section IV) with those of the 45 and 60 Mc/s plasma levels in type III source regions, we obtain the values of electron density plotted in Figure 13. In the same figure is given a third point (19·7 Mc/s) obtained by Shain and Higgins (1959) during a similar part of the current solar cycle, using a somewhat similar method. These points are shown in relation to the " normal " (Baumbach-Allen) coronal model and a model coronal streamer given by Newkirk (personal communication). The latter is based on many observations during the years 1956–1958 made with the white-light coronameter of the High Altitude Observatory, Boulder, Colorado. It is in close agreement with a detailed study of three streamers made by Schmidt (1953).

The radio values are seen to be an order of magnitude greater than the normal coronal densities. On the other hand they are similar to, though slightly greater than, those of the model streamer. This result suggests that type III disturbances may actually travel out along coronal streamers.

VI. The Distribution of Velocities

The results of Section IV led to the conclusion that the mean velocity of type III disturbances is of the order of $0{\cdot}5c$. The methods used were direct, but the conclusion depended to a great extent on the relatively small number of events which occurred near the limb. We now attempt to evaluate, necessarily by less direct means, the approximate radial velocity of each event, and hence arrive at a distribution of velocities.

For this purpose we shall assume that at a given frequency, f Mc/s, all bursts originate at the same radial distance, R_f, as in Figure 9. Using the values of R_{45} and R_{60} previously determined, the approximate radial component of velocity of a disturbance can be determined by

$$v=(R_{45}-R_{60})/(t_{45}-t_{60}).$$

When $v\sim c$, however, appreciable corrections are required to take account of the finite difference in the times taken by the two frequencies to propagate from their point of origin to the observer. The time delay then depends on the heliocentric angle α between the path of the disturbance and the Sun-Earth line (Fig. 9), and is given by

$$t_{45}-t_{60}=\left(\frac{1}{v}-\frac{1}{c}\cos\alpha\right)(R_{45}-R_{60})+\tau(\alpha),$$

SPEED OF TYPE III SOLAR RADIO DISTURBANCES

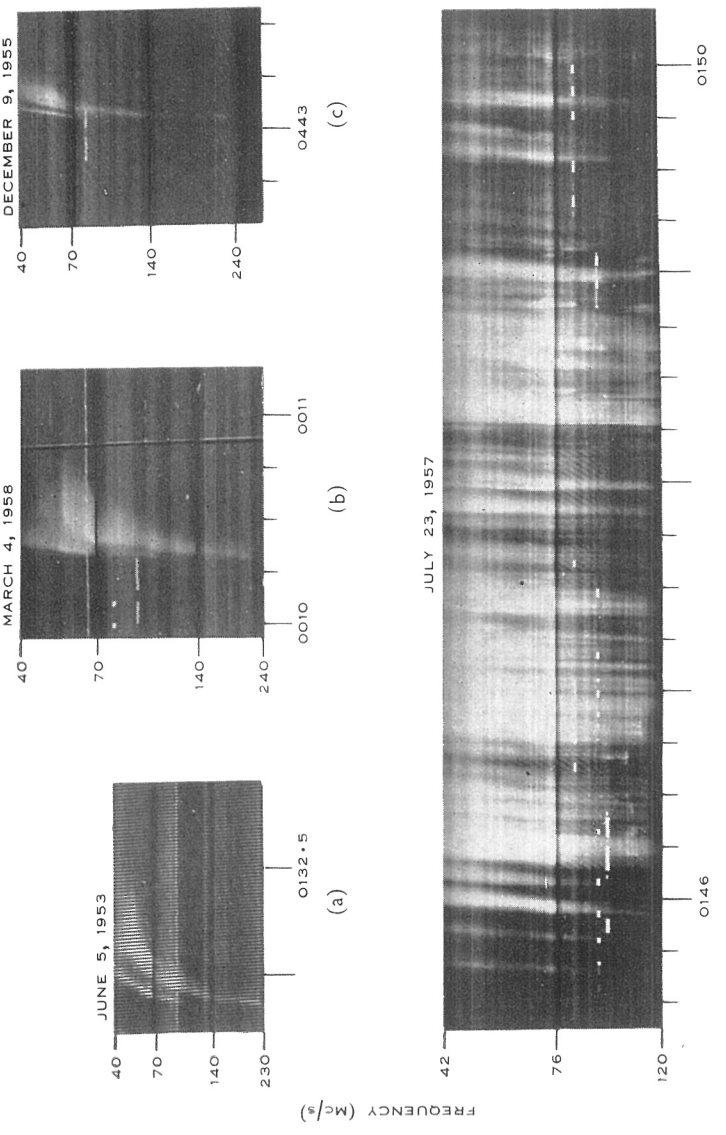

Examples of dynamic spectra of type III bursts. (*a*), (*b*), and (*c*) show individual bursts in which first and second harmonics can be recognized; (*d*) shows a typical large group of bursts. Scale of time: 4 divisions per min.

SPEED OF TYPE III SOLAR RADIO DISTURBANCES

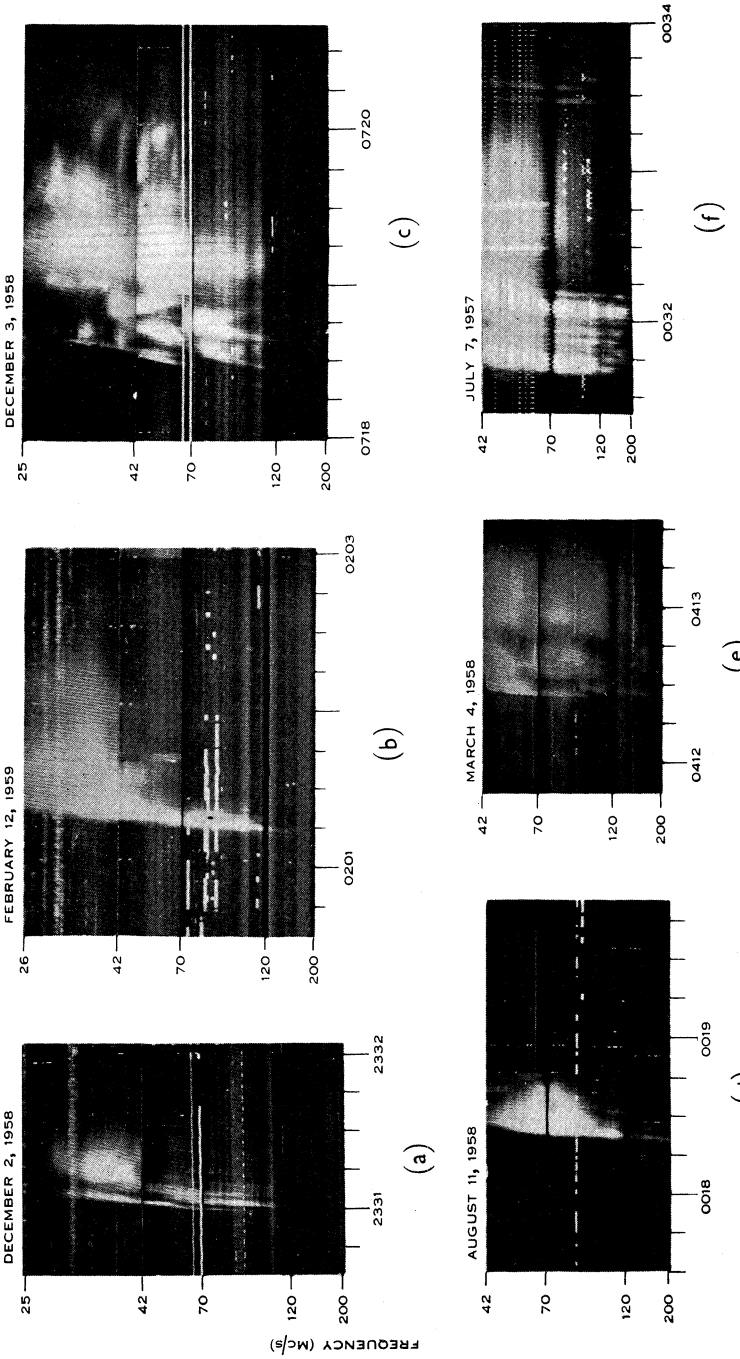

Examples of type III bursts which are followed by pronounced type V emission.

in which the first term on the right-hand side is obtained from simple geometric considerations on the assumption that the velocity of propagation is exactly c, and the second term $\tau(\alpha)$ is the correction required to allow for departures from this assumption. The correction $\tau(\alpha)$ can become appreciable when the path of propagation passes through regions whose refractive index departs significantly from unity (e.g. when the plasma hypothesis applies). Its evaluation is difficult and depends on the model atmosphere assumed. For the present purpose we calculate $\tau(\alpha)$ assuming that the propagation of each frequency can be regarded as rectilinear propagation through a spherically symmetrical atmosphere whose radial distribution of electron density is considerably greater than normal, viz. that given by the upper curve in Figure 14. Details of the calculation of $\tau(\alpha)$ are given in Appendix I, where an approximate analytical method is developed for treating the case of rectilinear propagation in any spherically symmetrical atmosphere. The adopted function $\tau(\alpha)$ is shown in Figure 16 in Appendix I.

For comparison with experimental data, we make use of the approximation*

$$P_{60} \approx R_{60} \sin \alpha,$$

and use the previous equation to plot values of $t_{45}-t_{60}$ as a function of P_{60} for various values of c (Fig. 14). Also to illustrate the effect of the badly known correction $\tau(\alpha)$, a curve corresponding to $v=c$ is given when $\tau(\alpha)$ is set equal to zero (dashed line).

On the same graph, each observed burst is represented as a closed or open circle. The latter refer to type III bursts which are confused by the presence of another form of emission (spectral type V) discussed subsequently.

While the observational points are widely scattered, the great majority lie between $P_{60}=0$ and $P_{60}=R_{60}$. The few points which lie outside this range are mainly subject to confusion by type V emission. We shall, of necessity, ignore these wayward points. In the main body of the diagram ($P_{60} \leqslant R_{60}$), there appears to be a significant upward sweep of points in the sense that both the mean and the minimum value of $t_{45}-t_{60}$ appear to increase with t_{60}. The same trend is present in the derived curves of constant velocity.

In this graph the abscissae of observational points are subject to errors of various kinds, e.g. the effects of refraction, non-radial paths, and limitations due to one-dimensional scanning. Inspection of the figure shows, however, that, except very near the limb, the determination of velocity is fairly insensitive to errors in the abscissae.

Figure 15 (full line) shows the distribution of the radial component of velocities derived directly from Figure 14. All points in the range $P_{60} \leqslant R_{60}$ were used, except two in which the derived velocity exceeded c. Owing to the uncertainty of the function $\tau(\alpha)$, a second distribution (dotted line) was evaluated setting $\tau(\alpha)=0$. The difference in the two distributions is slight except near the high velocity tail; this result means that the derived distribution does not

* This is strictly true only when the path of the disturbance lies in the same plane as the axis of the interferometer; it is approximately true for all radial disturbances originating at low heliographic latitudes.

critically depend on whether the radiation is supposed to originate at the fundamental plasma level or not.

The distribution shows a mean velocity of $0 \cdot 45c$. A striking feature is the abrupt low velocity cut-off at about $0 \cdot 2c$. The maximum velocity, whose determination is more hazardous, appears to lie within about 25 per cent. of the velocity of light.

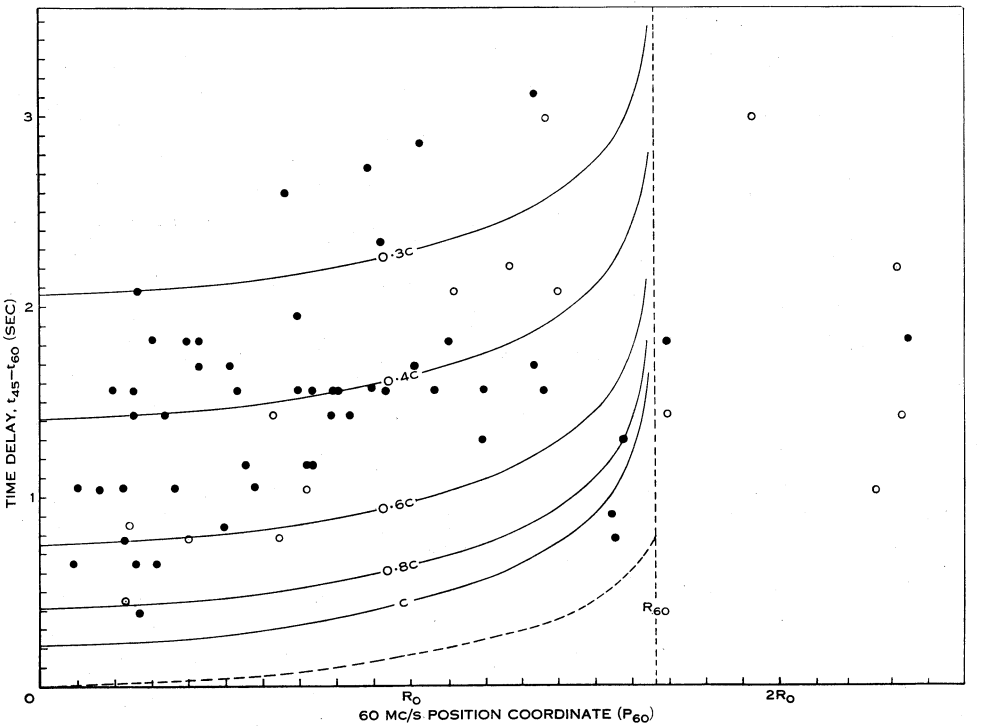

Fig. 14.—The distribution with 60 Mc/s position on the disk of the time interval between times of maximum intensity at 60 and 45 Mc/s for observed type III bursts. Each circle (full or open) represents an independent event. The curves show lines of constant velocity for type III disturbances, in terms of the velocity of light, c. These curves depend on assumptions described in the text. Those type III bursts which are followed by substantial type V emission are distinguished by open (as opposed to full) circles.

VII. Bursts of Spectral Type V

An important clue to the nature of type III disturbances is provided by a feature only briefly mentioned so far, namely, that certain type III bursts are followed by the broad-band diffuse afterglow known as the type V burst (Wild, Sheridan, and Trent 1959). The nature and origin of this emission will therefore be discussed before the origin of type III bursts is considered.

(*a*) *Description*

The type V burst may be defined as broad-band continuum radiation lasting for as long as 1 minute or more after a type III burst; appreciable type V emission occurs with perhaps 1 in every 3 or 4 groups of type III bursts. Examples of

type V spectra are given in Plate 2. In some cases the emission appears merely as a diffuse prolongation of the type III burst, in others as a detached blob or patchiness. The bursts radiate most strongly at frequencies below about 150 Mc/s, and sometimes the high frequency boundary has the form of a relatively sharp cut-off. The bandwidth is a substantial fraction of the mid frequency. Intensities as high as 10^{-18} W m^{-2} (c/s)$^{-1}$ are sometimes observed. No evidence of harmonic structure has been noted, and the spectra show no characteristics which suggest an origin in plasma oscillations. It is suggested that the type V emission is much more likely to be synchrotron radiation from relativistic electrons spiralling in the local magnetic field. A similar suggestion has been made by Boischot and Denisse (1957) to explain the type IV emissions which are also of broad bandwidth, but which follow type II bursts and persist for periods of hours.

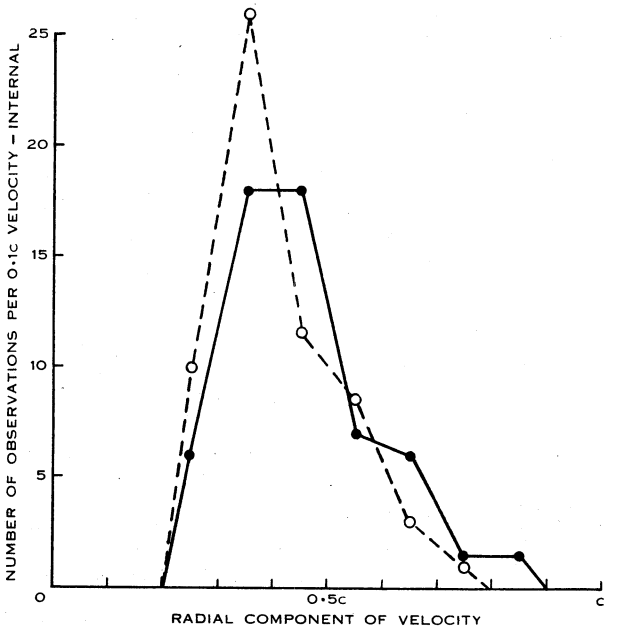

Fig. 15.—Distribution of velocities (radial component) of type III disturbances. The full line is derived directly from Figure 14; the dotted line shows the effect of neglecting the correction term $\tau(\alpha)$.

(*b*) *The Synchrotron Hypothesis*

To test the feasibility of the synchrotron hypothesis, we note that synchrotron radiation from an electron of energy E (MeV) spiralling with an angle of pitch Θ in a magnetic field of flux density B (gauss) shows a maximum in its spectrum at the frequency f_c, given by

$$f_c = 16BE^2 \sin\Theta \quad \text{(Mc/s)},$$

and that above this frequency the energy falls off rapidly. Hence, for $f_c = 100$ Mc/s, $BE^2 \approx 6$. Taking 1·5 G as a reasonable upper limit to the coronal magnetic field, and $\sin\Theta \sim 1$, we find that electron energies of at least 2 MeV are required.

The total power radiated by each electron is approximately $6\times10^{-22}B^2E^2\sin^2\Theta$ watts, and, assuming this power to be radiated in an effective bandwidth of $\frac{1}{2}f_c$, it can be calculated that the maximum flux density at the Earth due to each electron is

$$S=2\cdot7\times10^{-52}B\,\overline{\sin\Theta}\ \text{W m}^{-2}\,(\text{c/s})^{-1}.$$

Hence, neglecting self-absorption, the total number of electrons required to generate a flux density of 10^{-18} W m^{-2} (c/s)$^{-1}$ is

$$n=\frac{3\cdot7\times10^{33}}{B\,\overline{\sin\Theta}}$$
$$\gtrsim3\times10^{33},$$

since it may be assumed that $B\,\overline{\sin\Theta}\lesssim1\cdot2$. In the presence of self-absorption, rough thermodynamic arguments indicate that for electron energies of a few million electron-volts the radiating area of the source must be an appreciable fraction of the Sun's disk to yield the observed intensity ; this is supported by a preliminary source size measurement made at Dapto, where a value of 14 min of arc was obtained. We may therefore reasonably assume a radiating volume with linear dimensions of $\sim5\times10^5$ km, i.e. a volume of $\sim10^{32}$ cm^3. It follows that the required density of energetic electrons need be no greater than 30 cm^{-3}. A comparable figure (100 cm^{-3}) was deduced by Boischot and Denisse in their explanation of type IV bursts.

This brief discussion of type V bursts should be regarded as tentative in its quantitative aspects, since a detailed analysis of the observational material is required. In its support we may also mention a preliminary finding that the bursts are often polarized and that there are sometimes indications of linear polarization.

A number of the type III bursts used in the present analysis were accompanied by type V bursts. As previously mentioned, these are distinguished in Figure 14 by the open circles. While the number of cases shown is small, there appears to be a relatively higher probability for type V events to occur well away from the centre of the disk. This may imply that the magnetic fields tend to be radial, since synchrotron emission is beamed normal to the direction of the field. We may also note that events can occur far beyond the radio limb when synchrotron radiation is responsible for the emission.

VIII. On the Physical Nature of Type III Disturbances

Our interpretation of type V bursts requires the temporary existence high in the corona of a cloud of spiralling electrons with energy in excess of 2 MeV, i.e. with velocities within a few per cent. of the velocity of light. The minimum height at which radiation of a given frequency can escape is the corresponding plasma level. Thus, for example, the 45 Mc/s radiation in type V bursts would, according to our previous figures, originate at a radial distance of not less than $2R_0$. Now, it is known that many type V bursts, like the type III bursts that precede them, correlate very closely with the onset of chromospheric flares and sub-flares. We may therefore reasonably presume that the supply of fast electrons originates low in the solar atmosphere and that they are transported

with great rapidity to the heights whence the synchrotron radiation is emitted. Since the velocities of type III disturbances are found to be comparable with the velocity of light, it is extremely tempting to associate this act of transportation of the type V electrons with the type III disturbance. The fact that the majority of the type III disturbances are rather slower than the speed of million-volt electrons would be expected if the electrons travel along lines of magnetic force in a spiral path. Such electrons would travel through the corona practically unimpeded by collisions. We suggest specifically, therefore, that the disturbance responsible for initiating the plasma radiation in type III bursts is associated with a corpuscular stream ejected at the beginning of a flare and containing, in some cases at least, more than 3×10^{33} electrons with energy greater than 2 MeV. In some cases the electrons, following the magnetic field configuration, are returned to the Sun, giving rise to the variety of type III spectrum described by Maxwell and Swarup (1958) as the " inverted U " (see example in Plate 2 (*c*)). In other, more frequent, cases the electrons are guided out into interplanetary space, yielding the " normal " type III spectrum. It seems an attractive possibility that such electrons may be responsible for the corpuscular radiation round the Earth which has recently been observed with satellites (see, for instance, Van Allen 1959).

A possible objection to the theory is that the electron stream would pass too rapidly into the Sun or out of the solar atmosphere to explain the relatively long duration ($\sim$1 min) of the type V burst. It may therefore be necessary to postulate the existence of magnetic irregularities capable of trapping the type V electrons in the outer corona. Such irregularities would also ensure a supply of electrons with high pitch angles capable of generating synchrotron radiation near optimum power.

IX. Acknowledgments

Of the many members of the staff of the Radiophysics Laboratory who have contributed to the substance and preparation of this paper, the authors wish to thank particularly Mr. G. H. Trent, Mr. J. Joisce, and Mr. P. J. Collins for valuable assistance in assembling the equipment and in taking observations, Mrs. Marjorie Gorzkos for performing a large quantity of painstaking analysis, and Mr. K. R. McAlister and Mr. K. W. Anderson for the mechanical design of the computor and aerials. The authors also wish to thank Mr. C. A. Shain and Mr. D. J. McLean for helpful discussion and checking of the manuscript, and Dr. J. L. Pawsey for his interest in this work.

X. References

Boischot, A., and Denisse, J. F. (1957).—*C.R. Acad. Sci., Paris* **245**: 2194.
Giovanelli, R. G. (1958).—*Aust. J. Phys.* **11**: 350.
Hey, J. S., and Hughes, V. A. (1955).—*Mon. Not. R. Astr. Soc.* **115**: 605.
Hey, J. S., Parsons, S. J., and Phillips, J. W. (1948).—*Mon. Not. R. Astr. Soc.* **108**: 354.
Jaeger, J. C., and Westfold, K. C. (1950).—*Aust. J. Sci. Res.* A **3**: 376.
Komesaroff, M. (1958).—*Aust. J. Phys.* **11**: 201.
Loughhead, R. E., Roberts, J. A., and McCabe, Marie K. (1957).—*Aust. J. Phys.* **10**: 483.
Maxwell, A., and Swarup, G. (1958).—*Nature* **181**: 36.
Roberts, J. A. (1959).—*Aust. J. Phys.* **12**: 327.

SCHMIDT, M. (1953).—*Bull. Astr. Insts. Netherlds.* **12**: 61.
SHAIN, C. A., and HIGGINS, C. S. (1959).—*Aust. J. Phys.* **12**: 357.
VAN ALLEN, J. A. (1959).—*Nature* **183**: 430.
WILD, J. P. (1950).—*Aust. J. Sci. Res.* A **3**: 541.
WILD, J. P., and MCCREADY, L. L. (1950).—*Aust. J. Sci. Res.* A **3**: 387.
WILD, J. P., MURRAY, J. D., and ROWE, W. C. (1954).—*Aust. J. Phys.* **7**: 439.
WILD, J. P., ROBERTS, J. A., and MURRAY, J. D. (1954).—*Nature* **173**: 532.
WILD, J. P., and SHERIDAN, K. V. (1958).—*Proc. Inst. Radio Engrs., N.Y.* **46**: 160.
WILD, J. P., SHERIDAN, K. V., and TRENT, G. H. (1959).—I.A.U.-U.R.S.I. Symposium on Radio Astronomy, Paris 1958. p. 176. (Stanford Univ. Press.)

APPENDIX I

Evaluation of the Excess of Time, t, taken by a Radio-frequency Signal to escape along a Straight Path from its Plasma Level in a Spherically Symmetrical Ionized Atmosphere over that taken by Radiation travelling along the Same Path with the Velocity of Light

It is well known that the radial distribution of electron density, $N(r)$, in the solar corona can be simulated by an exponential function over a moderate range of r. Therefore, let the distribution be written in the form

$$N(r)=N_0 e^{-\beta(r)r}, \quad \ldots\ldots\ldots\ldots\ldots\ldots \quad (1)$$

where in cases of interest $\beta(r)$ is a relatively slowly varying function.

Let the point of origin of the disturbance be specified in polar coordinates (R,α), with the pole at the centre of symmetry and $\alpha=0$ directed along the path of escape (see Fig. 9). Take rectangular coordinates (x,y) through the centre, such that the x coordinate is directed along $\alpha=0$; then the path of the disturbance is given by

$$y=R\sin\alpha,$$

and

$$x^2=r^2-R^2\sin^2\alpha \quad (R\cos\alpha\leqslant x\leqslant\infty). \quad \ldots\ldots\ldots \quad (2)$$

The excess time is given by the integral

$$t=\frac{1}{c}\int_{R\cos\alpha}^{\infty}\left(\frac{1}{\mu}-1\right)\mathrm{d}x, \quad \ldots\ldots\ldots\ldots\ldots \quad (3)$$

where c is the velocity of light and the refractive index μ is given in terms of the plasma frequency

$$f_p=e(N/\pi m)^{\frac{1}{2}} \quad \ldots\ldots\ldots\ldots\ldots\ldots\ldots \quad (4)$$

(where e and m denote the electronic charge and mass), by

$$\mu^2=1-f_p^2(r)/f^2. \quad \ldots\ldots\ldots\ldots\ldots\ldots\ldots \quad (5)$$

In the present treatment we shall restrict ourselves to the case when the frequency is equal to the plasma frequency at $r=R$, namely,

$$f=f_p(R), \quad \ldots\ldots\ldots\ldots\ldots\ldots\ldots \quad (6)$$

but the treatment is capable of generalization to all frequencies. Combining equations (1), (2), (4), (5), and (6), we obtain the expression

$$x^2 = -R^2 \sin^2 \alpha + \{\beta(r)\}^{-2}\{\beta(R)R - \log(1-\mu^2)\}^2. \quad \ldots\ldots (7)$$

In using equation (7) to evaluate the integral (3), we shall assume that contributions towards the excess time come predominantly from a small range of r immediately above R, where the refractive index is small. This assumption is suggested by the computations of Jaeger and Westfold, and can be justified *a posteriori*. Hence, since $\beta(r)$ is a slowly varying function, we write $\beta(r)=\beta(R)\equiv\beta$, and equation (7) simplifies to

$$x^2 = -R^2 \sin^2 \alpha + \{R - \beta^{-1} \log(1-\mu^2)\}^2. \quad \ldots\ldots (8)$$

The central path.—Consider first the special case when the path of escape is along the x-axis ($\alpha=0$). Equations (3) and (8) then give

$$t = \frac{2}{\beta c}\int_0^1 \frac{d\mu}{1+\mu} = \frac{2\log 2}{c\beta}. \quad \ldots\ldots (9)$$

In practice the value of β is conveniently measured directly as a gradient in a plot of $\log N$ versus r. As an example, for the Allen-Baumbach model of the solar corona with $f=60$ Mc/s, we find $\beta(R)=5\cdot9R_0$, giving $t=0\cdot235R_0/c=0\cdot55$ sec. This value is some 15 per cent. lower than that computed by numerical integration by Jaeger and Westfold. However, the calculated *differential* time excess $t_{60}-t_{100}$ for the escape of 60 and 100 Mc/s signals from their respective plasma levels is found to agree with Jaeger and Westfold's value (approx. 0·08 sec) to within about 3 per cent. This example confirms what we might have expected intuitively—that the approximate method is more reliable for the calculation of differential values of time excesses as compared with absolute values.

General case.—For the general case ($0\leqslant\alpha\leqslant\frac{1}{2}\pi$), we write (8) in the form

$$x^2 = R^2\cos^2\alpha - 2R\beta^{-1}\log(1-\mu^2)[1-(2R\beta)^{-1}\log(1-\mu^2)].$$

In the solar atmosphere $2R\beta\sim15$, and μ is small in the region of interest. Hence we neglect the last term in the square brackets and obtain*

$$t \approx \frac{2R}{\beta c}\int_0^1 \{R^2\cos^2\alpha - 2R\beta^{-1}\log(1-\mu^2)\}^{-\frac{1}{2}}(1+\mu)^{-1}d\mu$$
$$\approx \frac{2R}{\beta c}\int_0^1 \{R^2\cos^2\alpha + 2R\beta^{-1}\mu^2\}^{-\frac{1}{2}}(1+\mu)^{-1}d\mu,$$

since $\log(1-\mu^2)\approx-\mu^2$ in the region of interest. This may be integrated using a substitution of the form $S=1+\mu$, and we obtain

$$t \approx 2(R/c)(2\beta R + \beta^2R^2\cos^2\alpha)^{-\frac{1}{2}}\log\{(1+2(\beta R)^{-1}\sec^2\alpha)^{\frac{1}{2}}+1\}. \quad .. (10)$$

* The fact that the neglected term exceeds $(2R\beta)^{-1}$ for values of $\mu>0\cdot8$, and indeed becomes infinite as $\mu\to1$, suggests that the upper limit of the integral should not be taken beyond about 0·8. However, it is found that doing so would scarcely affect the final value of t. This emphasizes the dominant role of the region of small μ values.

For the values used in this paper, the excess time delays computed from equation (**10**) for the central ray agreed with those computed directly from equation (**9**) to within about 5 per cent.

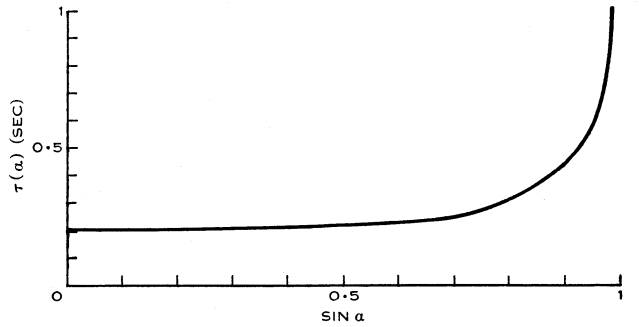

Fig. 16.

Application to particular case.—For the purposes of Section IV, we wish to evaluate the quantity

$$\tau(\alpha)=t(\beta_{45})-t(\beta_{60}), \quad \ldots\ldots\ldots\ldots\ldots \quad (11)$$

where β_{45} and β_{60} refer to the values of β at the 45 and 60 Mc/s plasma levels of the atmosphere whose radial distribution is given by the upper curve of Figure 13. It is found graphically that $\beta_1=3\cdot36/R_0$ and $\beta_2=4\cdot56/R_0$, and the corresponding values of R, as used in Section IV, are $R_{45}=2\cdot0R_0$ and $R_{60}=1\cdot66R_0$. Substituting in equations (**10**) and (**11**), we obtain the function $\tau(\alpha)$ shown in Figure 16.